

Geophysical Research Letters[®]

RESEARCH LETTER

10.1029/2022GL097779

Key Points:

- A machine-learning phase detector (EQTransformer) was applied to nearfield ocean bottom seismometer data at the southernmost Mariana trench
- The outer-rise seismicity at the southernmost Mariana trench varied along the trench, with one identified cluster
- We identified an outer-rise fault that penetrates to depths of 50 km

Supporting Information:

Supporting Information may be found in the online version of this article.

Correspondence to:

H. Yang,
hyang@cuhk.edu.hk

Citation:

Chen, H., Yang, H., Zhu, G., Xu, M., Lin, J., & You, Q. (2022). Deep outer-rise faults in the Southern Mariana Subduction Zone indicated by a machine-learning-based high-resolution earthquake catalog. *Geophysical Research Letters*, 49, e2022GL097779. <https://doi.org/10.1029/2022GL097779>

Received 13 JAN 2022

Accepted 2 JUN 2022

Deep Outer-Rise Faults in the Southern Mariana Subduction Zone Indicated by a Machine-Learning-Based High-Resolution Earthquake Catalog

Han Chen¹ , Hongfeng Yang^{1,2} , Gaohua Zhu^{1,3,4} , Min Xu^{5,6} , Jian Lin^{5,7,8} , and Qingyu You⁹

¹Earth System Science Programme, Faculty of Science, The Chinese University of Hong Kong, Hong Kong, China, ²Shenzhen Research Institute, The Chinese University of Hong Kong, Shenzhen, China, ³CAS Key Laboratory of Marine Geology and Environment, Center for Ocean Mega-Science, Institute of Oceanology, Chinese Academy of Sciences, Qingdao, China, ⁴Laboratory for Marine Geology, Qingdao National Laboratory for Marine Science and Technology, Qingdao, China, ⁵Key Laboratory of Marginal Sea Geology, Chinese Academy of Sciences, South China Sea Institute of Oceanology, Guangzhou, China, ⁶Southern Marine Science and Engineering Guangdong Laboratory (Guangzhou), Guangzhou, China, ⁷Department of Ocean Science and Engineering, Southern University of Science and Technology, Shenzhen, China, ⁸Department of Geology and Geophysics, Woods Hole Oceanographic Institution, Falmouth, MA, USA, ⁹Key Laboratory of Petroleum Resources Research, Institute of Geology and Geophysics, Chinese Academy of Sciences, Beijing, China

Abstract Outer-rise faults are predominantly concentrated near ocean trenches due to subducted plate bending. These faults play crucial roles in the hydration of subducted plates and the consequent subducting processes. However, it has not yet been possible to develop high-resolution structures of outer-rise faults due to the lack of near-field observations. In this study we deployed an ocean bottom seismometer (OBS) network near the Challenger Deep in the Southernmost Mariana Trench, between December 2016 and June 2017, covering both the overriding and subducting plates. We applied a machine-learning phase detector (EQTransformer) to the OBS data and found more than 1,975 earthquakes. An identified outer-rise event cluster revealed an outer-rise fault penetrating to depths of 50 km, which was inferred as a normal fault based on the extensional depth from tomographic images in the region, shedding new lights on water input at the southernmost Mariana subduction zone.

Plain Language Summary Estimating water input at subduction zones plays a crucial role in understanding the material cycles of the Earth and subduction zone dynamics. As outer-rise faults provide the primary channel for water to penetrate into the incoming plate, investigating the generation and extent of outer-rise faults is thus an effective way to understand the hydration degree. However, high-resolution structure of outer-rise faults is not common due to the lack of near-field observations. In this study, we apply a machine-learning phase detector (EQTransformer) to a new ocean bottom seismometer data set at the southernmost Mariana Subduction Zone. After careful analysis of earthquake location and clustering, we find a deep outer-rise fault extending to 50 km in depth. We interpret the fault as a normal fault based on the depth range of a cluster of events with high waveform similarity. Such a deep outer-rise fault implies much higher water input at southernmost Mariana than had been previously estimated.

1. Introduction

Subducting plates bulge and bend near trenches in the outer-rise region, leading to extensional and compressional stress regimes in the upper and lower regions, respectively, which are separated by a neutral plane (Chapple & Forsyth, 1979). It is generally accepted that the extensional stress may generate outer-rise normal faults, some of which have extended to the seafloor (Hilde, 1983; Jones et al., 1978). Indeed, prevalent bending-related faults, as evidenced by bathymetric data and multi-channel seismic (MCS) reflection profiles, have been observed in various subduction zones, including the Java Trench (McCaffrey et al., 1985), the Tonga Trench (Lonsdale, 1988), the Chile Trench (Ranero et al., 2005), the Japan Trench (Kobayashi et al., 1987; Renard et al., 1987), the Middle American Trench (Moore & Shipley, 1988; Shipley & Moore, 1985), and the Peru Trench (Warsi et al., 1983). According to these observations, outer-rise faults are often found within distances of ~75 km from the trench axis. The faults are typically 5–30 km long with an inter-fault distance of 1–10 km, with the fault throws gradually decreasing seaward (Masson, 1991). Although the faults tend to form in a relatively narrow region, the deformation caused by

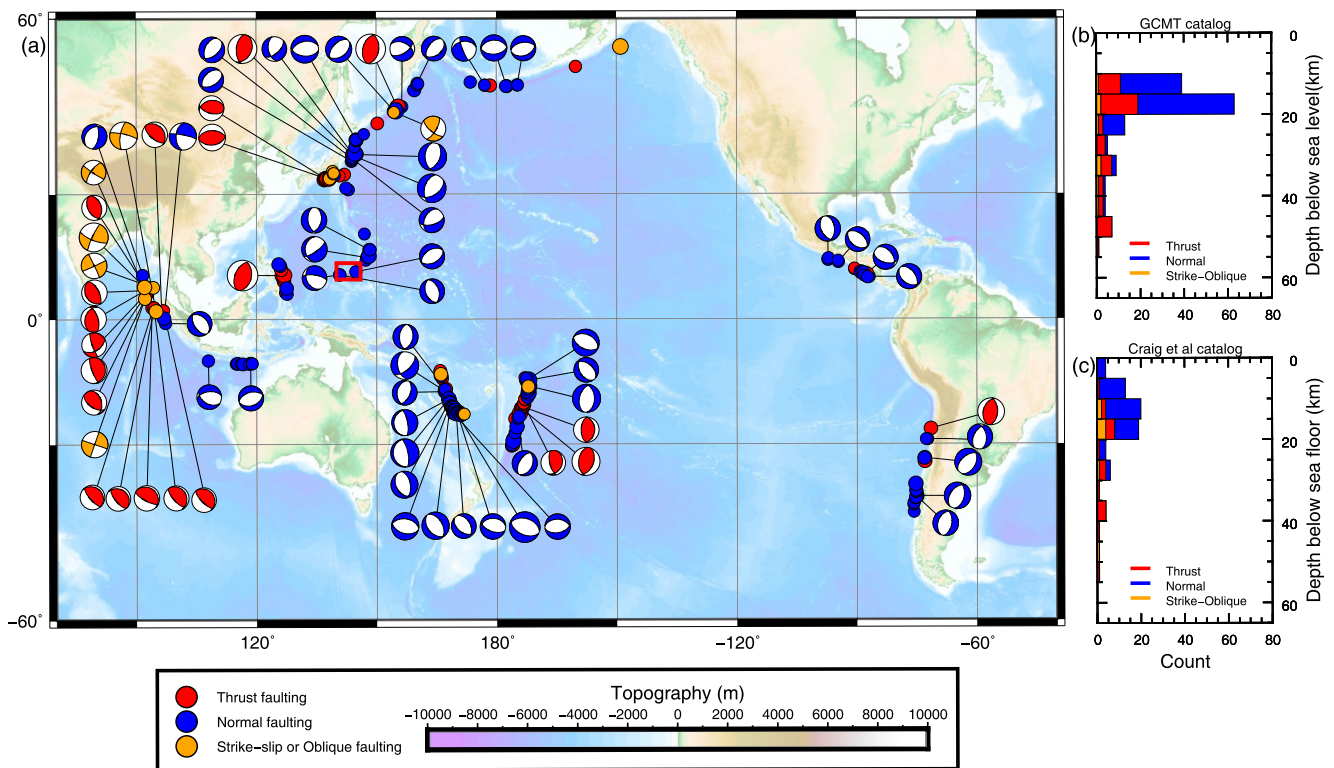


Figure 1. Global Outer rise seismicity. (a) Global outer-rise seismicity with magnitudes larger than Mw 6.0 from 01 January 1976 to 12 December 2021. Outer-rise earthquakes with accurately constrained source parameters (catalog comes from (Craig & Copley, 2018; Craig et al., 2014)) are marked in various colored focal mechanism plots, according to their mechanism, thrust faulting - red; normal faulting - blue; strike-slip or oblique faulting - orange. Outer-rise events from GCMT Catalog are given by colored circles, the colors share the same meaning as the catalog from references. We modified the GCMT catalog by removing the events that same as the reference catalog. The red box represents the study region of this research. (b) The stacked histogram of the depth distribution of outer-rise seismicity in the modified GCMT catalog. The area of colored patches is proportional to the event number. (c) Shares the same meaning as panel (b), but for catalog comes from (Craig & Copley, 2018; Craig et al., 2014).

fault activities significantly influences the distribution of outer-rise earthquakes (Christensen & Ruff, 1988; Jiao et al., 2000; Ranero et al., 2005; Stauder, 1968) and oceanic plate hydration (Peacock, 2001; Ranero et al., 2003).

Incoming plates at subduction zones are the major regions where water can be transferred into the Earth's depths. Estimating the degree of hydration of the incoming plates usually requires high-resolution tomographic images based on near-field observations (Cai et al., 2018; Fujie et al., 2013; Shillington et al., 2015; Van Avendonk et al., 2011; G. Zhu et al., 2021). Since the outer-rise normal faults serve as pathways for water penetrating into the oceanic plate before subduction (Grevemeyer et al., 2007; Ivandic et al., 2010; Peacock, 2001; Ranero et al., 2003), the depth extent of outer-rise normal faults has been regarded as a good indicator of the water input in the subduction zones. MCS reflection profiles have been used to determine the extent of faults, and it has been recognized that the outer-rise faults sometimes cut through the crust and reach the upper mantle (Ranero et al., 2003). In addition, focal depths of outer-rise earthquakes have been commonly used as proxies for the deep extent of faults. The global outer-rise earthquake depths indicate that the normal faults penetrate around 20–25 km beneath the seafloor and reach the upper mantle (Figure 1) (Christensen & Ruff, 1988; Craig et al., 2014; Emry & Wiens, 2015). Numerical models of plate bending have also been developed to derive the yielding depth of the incoming plate, which is often used to infer fault depth extent and thus hydration degree of the plate (Hunter & Watts, 2016; F. Zhang et al., 2018; J. Zhang et al., 2021, 2022; Z. Zhou et al., 2015). However, a large number of outer-rise regions have so far been poorly investigated, because of the lack of available data. Detailed investigations relying on near-field observations through the deployment of ocean bottom seismometers (OBSs) are therefore important.

High-resolution seismic tomographic images derived from recent OBS experiments in the Southern Mariana Subduction Zone indicate hydration of the upper mantle near the trench (Wan et al., 2019; G. Zhu et al., 2021).

Numerous outer-rise faults have been observed in the region, as shown in bathymetric data (Fisher, 1974; Nakanishi & Hashimoto, 2011; Z. Zhou et al., 2015), but the depths of these faults have yet to be determined. Given the constraints of the bathymetric data, numerical models have been developed to estimate the normal faulting in the Southern Mariana Trench. For example, Z. Zhou et al. (2015) conducted 2-D elastoplastic modeling and suggested that the maximum depth extent of outer-rise normal faults in the trench was around 30 km below the seafloor, close to the depth of serpentinization within the incoming plate that was inferred from tomographic results (G. Zhu et al., 2021). The focal depths of extensional earthquakes have also been used as indicators. Emry et al. (2014) located several extensional outer-rise earthquakes by inverting teleseismic *P* and *SH* waveforms, indicating a maximum focal depth of 12 km below the seafloor in the Central Mariana Trench, while Eimer et al. (2020) located incoming plate events with depths of ~35 km below the seafloor in the same region using near-field OBS data. The inconsistent results of such studies indicate the high degree of uncertainty inherent in investigating outer-rise faults. Similarly, a local earthquake catalog in the Southern Mariana Trench from a near-field OBS data set revealed outer-rise seismicity with a maximum depth of ~40 km (G. Zhu et al., 2019). However, the vertical margin of error in their estimate of outer-rise seismicity could have amounted to several tens of kilometers, because the OBS network used in their study was located only on the overriding plate. The features of the outer-rise faults and the effects of along-trench variations of the plate on the development of the outer-rise faults remain unclear.

In this study, we use data recorded by the OBS network that covered both the subducting and the overriding plates in the Southern Mariana Subduction Zone to investigate outer-rise seismicity and faults (Figure 2). We first identify and pick *P*- and *S*-wave phases by using a machine-learning phase picker—EQTransformer (Mousavi et al., 2020) and associate detected phases using the Rapid Earthquake Association and Location (REAL) algorithm (M. Zhang et al., 2019). We then locate the associated events using the Hypoinverse (Klein, 2002) and refine the location using the HypoDD program (Waldhauser & Ellsworth, 2000). The newly relocated outer-rise earthquakes provide constraints on the distribution and depth extent of the outer-rise faults.

2. Tectonic Setting

The Mariana Subduction Zone is located at the boundary between the eastern edge of the Philippine Sea Plate and the subducting Pacific Plate (Figure 2). Subduction along the boundary began in the Eocene prior to about 52 Ma (Arculus et al., 2015). The Mariana Trench migrated toward the east, relative to the West Philippine Sea Plate, due to the rolling back of the subducted plate. The geometry of the subduction system became bowed out eastward as the subducting plate rolled back, while it was pinned at the northern and southern ends of the trench system by the impinging Ogasawara Plateau and Caroline Ridge, respectively (Hsui & Youngquist, 1985; Moberly, 1972). The Central and Southern Mariana Troughs experienced different opening modes. Magmatic seafloor spreading was relatively focused in the Central Mariana Trough, but the spreading at the southern end of the trough was more diffuse (Sleeper et al., 2021). Subduction behaviors were also different along the trench under the influence of the geometry and the opening modes of the subduction system. For example, significant inclination changes of the subducted plate have been observed at the trench axis (Oakley et al., 2008; Z. Zhou et al., 2015).

The Mariana Subduction Zone is generally regarded as a water-rich system, based on the wide distribution of serpentinite mud volcanoes in the forearc and the observed serpentinized upper mantle (Fryer et al., 1999; Pozgay et al., 2009; Pyle et al., 2010). Bathymetric data shows that outer-rise normal faults are predominantly distributed in this subduction zone. Most of these outer-rise normal faults begin to develop at around 60–100 km from the trench axis (Oakley et al., 2008; Z. Zhou et al., 2015). Widely distributed outer-rise faults have promoted water penetration into the subducted plate and consequent plate hydration. Seismic images of the Central and Southernmost Mariana Trench have revealed a serpentinized uppermost mantle beneath the subducted plate (Cai et al., 2018; Wan et al., 2019; G. Zhu et al., 2021).

3. Data and Methods

The data used in this study was collected by two passive-source OBS experiments that were conducted near the Challenger Deep, which ran across the Southernmost Mariana Trench. Seven OBSs were deployed and 6 were recovered in the first experiment, which was conducted from 15 December 2016 to 12 June 2017, and 6 OBSs

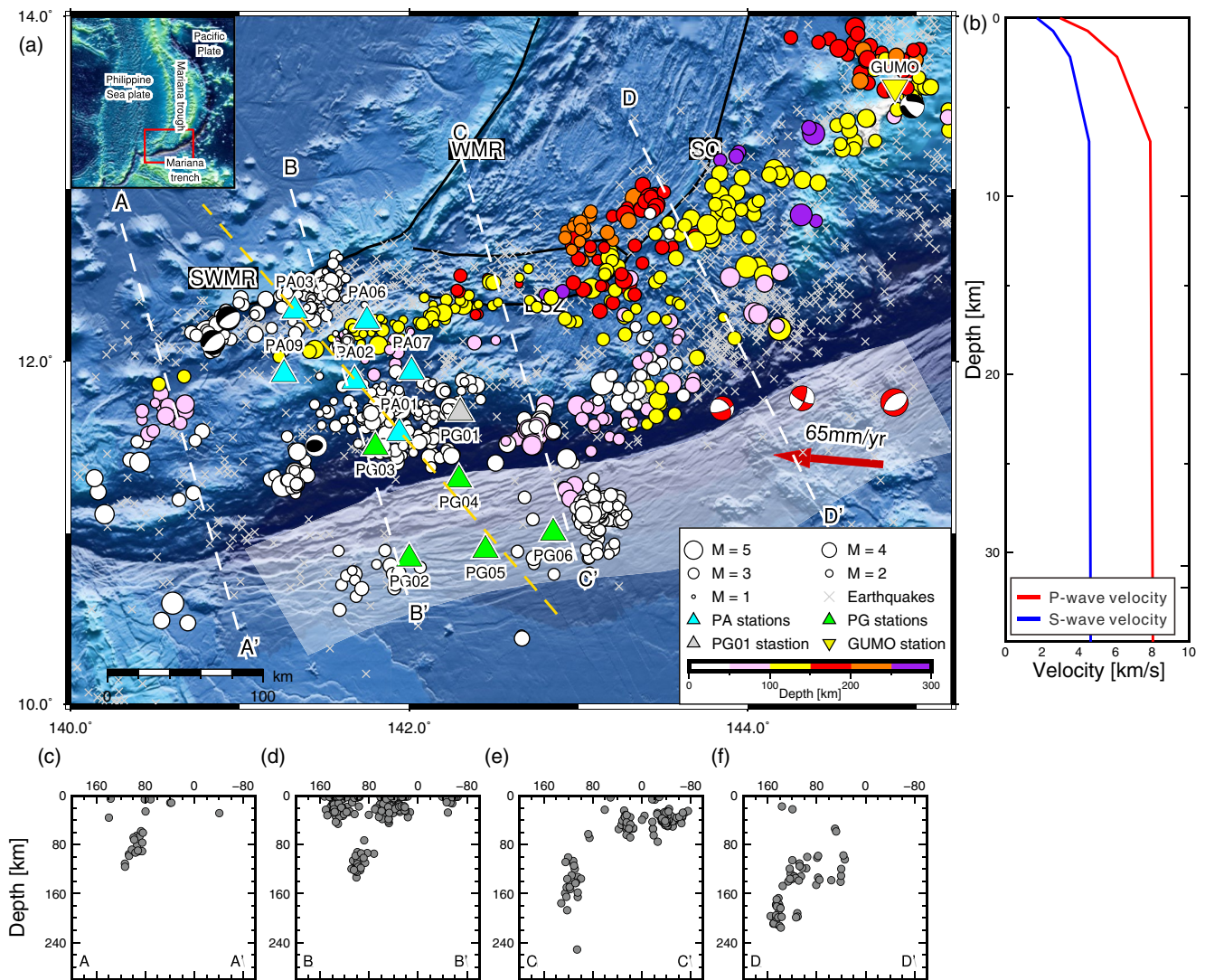


Figure 2. (a) The locations of ocean bottom seismographs (OBSs) are indicated by triangles. Cyan triangles denote OBSs deployed from 28 February 2017 to 12 June 2017, while green ones show long-term OBSs deployed between 15 December 2016 and 12 June 2017. The yellow triangle represents the GUMO station. The HypoDD located earthquakes were plotted as circles that were colored by depth. The red focal mechanism plots denote outer-rise earthquakes reported by Emry et al. (2014), while the black focal mechanism plots denote earthquakes reported by GCMT during the period of OBSs deployment. The gray crosses represent earthquakes with magnitudes larger than 5 in the ISC catalog from 1962 to 2021. The dashed gold line represents the active air-gun source ocean bottom seismometer profile (Wan et al., 2019), while the dashed white lines represent the cross-sections. The outer-rise region was roughly marked by the white-filled polygon. (b) The velocity model we used in relocation. Red and blue lines represent the *P*-wave and *S*-wave velocities, respectively. (c, d, e, and f) Cross-section views of seismicity (gray dots) with a bin width of 30 km. Trench locations are marked as 0 km.

were deployed and recovered in the second experiment, which was carried out from 28 February 2017 to 12 June 2017 (Figure 2). The OBS time errors were corrected based on both teleseismic waveforms and ambient noise cross-correlation (CC) (G. Zhu et al., 2019). The orientation and polarity of the OBSs were corrected via polarization analysis and waveform modeling (G. Zhu et al., 2020). Except for the PG01 station, which was only included in phase detection because of its irregular time shift (G. Zhu et al., 2020), all other OBSs were used in both earthquake detection and location in this study.

We adopted EQTransformer (Mousavi et al., 2020) in the earthquake phase picking and the REAL method (M. Zhang et al., 2019) to associate the detected phases. We located the detected earthquakes by the HypoInverse-2000 program (Klein, 2002) and further improved the earthquake locations using the double-difference relocation algorithm (HypoDD) (Waldhauser & Ellsworth, 2000). The seismogenic fault of the outer-rise cluster was identified based on the locations of events with high similarity in waveforms.

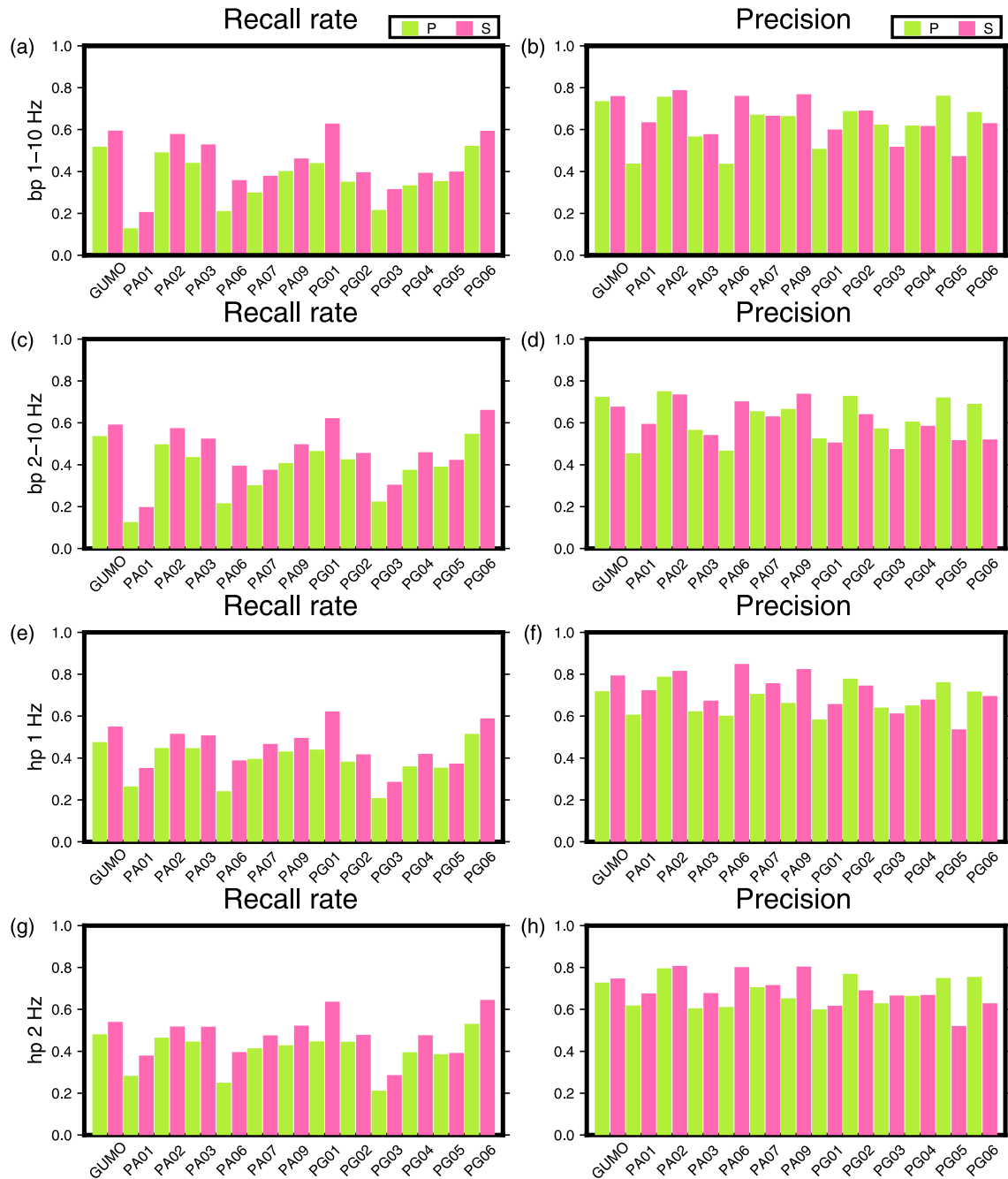


Figure 3. The recall rate and precision of EQTransformer while applying to ocean bottom seismometer data with different filter bands. (a) shows the recall rate and (b) shows the precision of EQTransformer on a 1–10 Hz bandpass filtered data. (c and d), (e and f), and (g and h) are recall rates and precisions for 2–10 Hz band-pass filtered, a 1 Hz high-pass filtered, and a 2 Hz high-pass filtered data, respectively. Green and pink bars represent P picks and S picks, respectively.

4. Results

4.1. Earthquake Phase Detection and Association

We first examined the performance of PhaseNet (W. Zhu & Beroza, 2019) and EQTransformer (Mousavi et al., 2020) on our test OBS data set (pre-obtained 1,461 event waveforms with manual labeled *P*- and *S*-wave arrivals) with various frequency bands (Text S1 in Supporting Information S1). The result showed that the performance is the best (i.e., with the highest recall and precision rate) on 1-Hz high pass filtered data for both methods (Figures 3 and S4 in Supporting Information S1). Although the recall rate of EQTransformer is lower than

PhaseNet, EQTransformer reported fewer false positives. We thus adopted The EQTransformer and 1 Hz high pass filter in our three-components continuous data for phase picking.

We then associated the detected phases by REAL. The searching range was set as 2° around the OBS station which recorded the first signal of an event, with a grid size of 0.1° . The searching depth ranged from 0 to 300 km, with a grid size of 10 km. The thresholds of the *P*, *S*, and total arrival numbers were set as 3, 0, and 5 for the data from 1 January 2017 to 3 May 2017 (only PA stations deployed) and 4, 0, and 6 for the data from 4 May 2017 to 13 June 2017 (both PA and PG stations deployed). The velocity model we used in the REAL association is the IASP91 global velocity model (Kennett & Engdahl, 1991). In total, 24,403 *P*-phases and 26,160 *S*-phases were picked in the continuous data. 17,273 out of 50,563 phases were associated, forming 1,975 events with initial locations.

4.2. Earthquake Relocation

The detected earthquakes were first located by the Hypoinverse method, in which a hypoellipse velocity model that counted station elevation during inversion (Klein, 2002) was adopted to eliminate the influence of the large variation in OBS elevations. Here we used a newly constructed velocity model (Figure 2b), which incorporated a more accurate shallow velocity structure obtained through an active source OBS experiment across the Challenger Deep (Wan et al., 2019). Below 7 km we still used the IASP91 global velocity model (Kennett & Engdahl, 1991).

The locations were then refined by the HypoDD method, utilizing both catalog and CC differential times. The catalog differential times were calculated directly based on the *P*- and *S*-wave picks. The CC differential times were obtained through waveform CC on 0.5–4 Hz bandpass filtered three-components data (Yang et al., 2009) with a CC coefficient threshold of 0.6. We conducted 25 iterations in HypoDD location, with strong weighted (1.0 for *P*-wave and 0.5 for *S*-wave) catalog differential times and weak weighted (0.1 for *P*-wave and 0.1 for *S*-wave) CC differential times during the first 10 iterations, and a reversed weighting strategy during the latter 15 iterations, to properly combine the two sets of differential times and resolve both large- and small-scale distribution characteristics of the events.

1,972 out of 1,975 earthquakes were relocated by Hypoinverse (Figure S1 in Supporting Information S1) and 898 earthquakes were then relocated by HypoDD (Figure 2). The located slab-related earthquakes suggest that the length and dip angle of the subducted plate length increased from the west to the northeast. Furthermore, the seismicity in the outer-rise region clearly varies along trench although normal faults were pervasively distributed, with an events cluster close to OBS PG06 and a seismicity gap remaining between PG02 and PG06 stations. The maximum depth of the outer-rise cluster extended to ~ 50 km, while the depths of the isolated outer-rise events were mostly less than 30 km. Moreover, the back-arc seismicity is limited toward the southern end of WMR, with numerous shallow earthquakes, and nearly no earthquake occurring to the north.

4.3. Outer-Rise Fault Identification

A seismogenic fault was identified based on the outer-rise sub-cluster events. We first relocated the outer-rise events, bounded by latitudes $[10^\circ\text{N}–11.5^\circ\text{N}]$ and longitudes $[142.5^\circ\text{E}–143.5^\circ\text{E}]$, specifically. We inspected and corrected the phases of the outer-rise events manually and labeled phases that were missed, and relocated the cluster events following the same processes above. We then conducted waveform CC on data recorded by the closest PG06 station in a filter band of 0.5–8 Hz and a time window 0.5 s before and 2.5 s after the *S*-wave arrival to search for sub-clusters with highly similar waveforms. The CC coefficient matrix (Figure S2 in Supporting Information S1) showed an obvious clustering feature of the outer-rise cluster. The outer-rise cluster was thus separated into sub-clusters based on the waveform CC coefficient. For each event (the template), we searched for and counted the number of events with CC coefficients large than 0.7 to form sub-clusters. We then determined the outer-rise fault plane by visually inspecting the cross-sections of the sub-cluster with the largest event number.

The location uncertainties were estimated from the bootstrapping (Billings et al., 1994) and jackknife methods (Tichelaar & Ruff, 1989). In the bootstrapping process, random errors following normal distribution were added

to the arrival times in each HypoDD iteration. The normal distribution parameters ([*P*-wave: $\sigma = 0.33$ and $\mu = 0.015$] and [*S*-wave: $\sigma = 0.265$ and $\mu = 0.111$]) were obtained based on the time residual between manual (from the test OBS data set) and EQTransformer picks (Figure S6 in Supporting Information S1). In the jackknifing process, 90% of the differential time pairs (both catalog and CC differential times) were randomly selected and used in each HypoDD iteration. We repeated both the bootstrapping and jackknife processes 300 times and estimated the uncertainties as the double standard deviations (2σ) of the locations. Because of the limited spatial coverage of our OBS network, the outer-rise cluster was located to the east of stations. We also evaluated the influence of the large azimuth gap resulting from the relative location between the cluster and the OBS network by relocating synthetic events. Our results showed that the relative position between the network and events had little influence on the HypoDD location result. The details are included in Text S2 in Supporting Information S1.

The relocated outer-rise cluster included 101 events and was centered on longitude 143.09°E and latitude 11.09°N, with a depth range of 20–55 km (Figure 4). We obtained a sub-cluster with highly similar waveforms (Figure S3 in Supporting Information S1), which delineated an outer-rise fault. The projection of sub-cluster events to the BB' cross-section (strike -50° N) showed a clear linear trend while projection to AA' cross-section (strike 40° N) was more scattered, indicating a seaward dipping fault plane with a strike of 40° N, ranging from 20 to 50 km below the seafloor (Figures 4a–4c). The absolute horizontal (E-W and N-S directions) and vertical location uncertainties of all outer-rise events in different depths were calculated, with conservative estimate values less than 5 and 10 km, respectively (Figures 4d–4f), because the generated error pool was more scattered than the data (Figure S6 in Supporting Information S1). The relative location uncertainties of sub-cluster events were mostly less than 1 km in horizontal (E-W and N-S direction) and 2 km in vertical directions (Figures 4g–4i).

5. Discussion

5.1. Machine Learning Method Application on OBS Data

To the best of our knowledge, this is the first study in which machine learning algorithms have been applied to OBS data in the Southern Mariana Trench. The machine learning algorithm detected local earthquakes with a high degree of accuracy on our OBS network data, with most of the newly detected earthquakes being small magnitude ($M < 3$) events that were missed by global stations (Figure 2 and S1 in Supporting Information S1). The newly detected outer-rise earthquakes provided constraints on the depth extent of outer-rise faults.

Although machine learning methods are powerful in handling massive amounts of seismic data in a short time, no model trained based on OBS data is available now. We tried to transfer training the PhaseNet model based on our event data set (see details in Text S3 in Supporting Information S1) but did not find significant improvement due to the limited event numbers in the training data set. If sufficient OBS data could be collected and utilized, a better machine learning model for OBS data could be obtained in the future.

5.2. The Generating Modes of the Identified Fault

The strike of outer-rise faults is an important parameter in determining whether the faults are reactivated seafloor fabrics or newly generated faults (Billen et al., 2007; Henza et al., 2010; Masson, 1991; Ranero et al., 2005). The located outer-rise sub-cluster depicts a fault plane with a strike of around 45° , which is subparallel to the magnetic line in the Southernmost Mariana Trench (Figures 4a and 4c), suggesting a generating mode of inherited seafloor fabrics reactivation.

Observations (Masson, 1991; Ranero et al., 2005) and experimental model simulations (Henza et al., 2010) show that the angle between the pre-existing weakening zones (inherited seafloor fabrics) and the trench axis controlled the development of the outer-rise faults. Reactivation of inherited seafloor fabrics and the generation of new faults may coexist when the angle is around 30° (Masson, 1991). In the study region, the magnetic lines are with angles about 30° to the trench axis and the fault scarp shown in the bathymetry data, indicating that reactivation of inherited seafloor fabrics and generation of new faults may both exist. Thus, we conclude that the identified outer-rise fault was a reactivated inherited seafloor fabric.

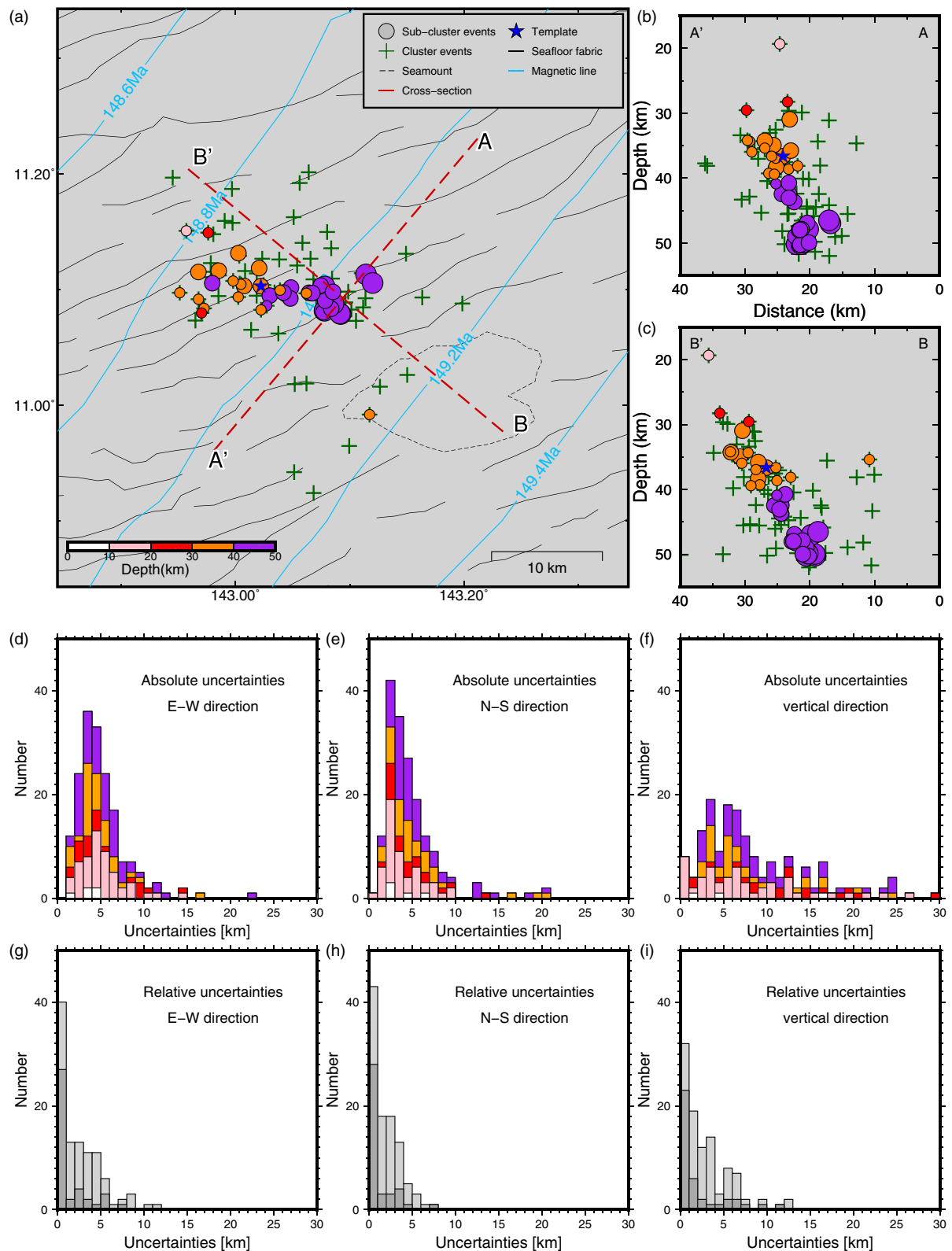


Figure 4. (a) HypoDD locations of the outer-rise cluster (green crosses) and sub-cluster events (circles colored by depth). The cross-section view of the earthquakes aligned (b) parallel and (c) perpendicular to the magnetic line, respectively. (d–f) Absolute (Hypoinverse) location uncertainties in E–W, N–S, and vertical directions, respectively. Colors indicate event depths. (g–i) Relative (HypoDD) location uncertainties in E–W, N–S, and vertical directions, respectively. Light-gray bars represent all the outer-rise cluster events and dark-gray bars represent the sub-cluster events.

5.3. The Depth Extent and Faulting Type of the Identified Fault

Studies have demonstrated that the hydration of subducting oceanic plates mostly occurs in the outer-rise region, where normal faults are widely distributed (Cai et al., 2018; Peacock, 2001; Ranero et al., 2003; G. Zhu et al., 2021). The depth extent of outer-rise faults determines how deep the fluid can penetrate into the plate, and is, therefore, an important factor in estimating the hydration degree of the plate. Based on the earthquake location, we infer that the depth extent of the identified fault is around 50 km beneath the seafloor, much deeper than the extensional yield zone (~30 km) derived from elastoplastic model simulations (Z. Zhou & Lin, 2018; Z. Zhou et al., 2015).

The global outer-rise normal fault earthquakes are generally shallower than 20–25 km beneath the seafloor (Christensen & Ruff, 1988; Craig et al., 2014). However, some studies have also reported outer-rise normal fault events at larger depths, such as the Mw 7.2 earthquake in the Aleutian Trench in 1965 (Abe, 1972) and the Mw 8.3 normal earthquake in the Sumba Trench in 2012 (Lynnes & Lay, 1988). Ward (1984) suggested that additional regional stresses in an elastic bending plate model could change the depth of the neutral plane with a magnitude of 20 km without significant changes in plate profile and maximum internal stress. The 3-D plate bending model in the Southernmost Mariana Trench shows a significant variation of bending stress in the identified fault position due to the trench-parallel variation of plate bending deformation (J. Zhang et al., 2020), which might have changed the neutral plane depth in the region and resulted in a deep outer-rise fault.

We attempted to determine the focal mechanisms of large sub-cluster earthquakes ($M > 4$) to determine the fault type. We first conducted a focal mechanism inversion by using the Cut and Paste (CAP) waveform modeling method (L. Zhu & Helmberger, 1996). However, we were unable to robustly recover the focal mechanisms (Figure S10 in Supporting Information S1). Because of the limited station coverage, the resolutions were limited even when we used synthetic waveforms. Besides the CAP method, we also used HASH, a method of obtaining focal mechanism solutions based on P -wave first motion polarity. However, due to the large azimuth gap (nearly 270°) and limited clear P -wave onset records, the inversion results had no resolution at all (Figure S12 in Supporting Information S1). We also tried to determine the rake of the identified outer-rise fault by the waveform forward modeling, in which we compare the real data with the synthetic waveforms that were generated based on the fault geometry and various rakes (0–360°). However, no optimal rake was found. Details of these attempts are included in Texts S4, S5, and S6 in Supporting Information S1.

The newly constructed SV -wave velocity model of the study region demonstrates serpentinization extending to a depth of ~32 km below the seafloor (G. Zhu et al., 2021), indicating that the extensional stress region and the extent of normal faults may extend to a greater depth. The extensional stress region in the study region obtained from numerical modeling also extends to ~30 km in depth (F. Zhang et al., 2018; J. Zhang et al., 2021; Z. Zhou et al., 2015). Because the sub-cluster events span in depths of 20–50 km, we thus infer the identified fault as a normal fault.

Unfortunately, we are unable to conclude whether the deep outer-rise fault is ubiquitous in southern Mariana because of the limited station coverage. However, if such normal faults with a large depth extent are widespread in the outer-rise, the water input in the Southern Mariana subduction zone will be higher than what has been previously estimated. Further investigations are needed to obtain the whole picture of outer-rise faults at the southernmost Mariana subduction zone.

6. Conclusion

We applied the machine-learning-based earthquake detection method to a new OBS data set at the southernmost Mariana subduction zone and found nearly 2,000 earthquakes. The seismicity in the outer-rise region varies along the trench, with an outer-rise earthquake cluster identified. The outer-rise sub-cluster depicted a normal fault, resulting from the reactivation of the inherited seafloor fabrics, that penetrated to a depth of 50 km. This result indicated that there might be larger water input in the Southern Mariana Subduction Zone than had previously been estimated.

Data Availability Statement

The relocated event waveform data are available online (<https://doi.org/10.6084/m9.figshare.18266960.v2>).

Acknowledgments

The authors are grateful to the science parties and crew members of the R/V Shiyuan 3 and the Tansuo 1 for the deployment and collection of the ocean bottom seismometer instruments. This study is supported by National Natural Science Foundation of China (Nos. 91858207, 92158205, 41890813), Hong Kong Research Grant Council Grants (No. 14304820), Award from CORE (a joint research center for ocean research between QNLM and HKUST), Chinese Academy of Sciences (Nos. Y4SL021001, QYZDY-SSW-DQC005), and Southern Marine Science and Engineering Guangdong Laboratory (Guangzhou) (No. GML2019ZD0205), Faculty of Science at CUHK. We thank the editor and two anonymous reviewers for their constructive comments that help improve the paper.

References

- Abe, K. (1972). Focal process of the South Sandwich Islands earthquake of May 26, 1964. *Physics of the Earth and Planetary Interiors*, 5, 110–122. [https://doi.org/10.1016/0031-9201\(72\)90080-5](https://doi.org/10.1016/0031-9201(72)90080-5)
- Arculus, R. J., Ishizuka, O., Bogus, K. A., Gurnis, M., Hickey-Vargas, R., Aljehdali, M. H., et al. (2015). A record of spontaneous subduction initiation in the Izu–Bonin–Mariana arc. *Nature Geoscience*, 8(9), 728–733. <https://doi.org/10.1038/ngeo2515>
- Billen, M., Cowgill, E., & Buer, E. (2007). Determination of fault friction from reactivation of abyssal-hill faults in subduction zones. *Geology*, 35(9), 819–822. <https://doi.org/10.1130/g23847a.1>
- Billings, S., Sambridge, M., & Kennett, B. (1994). Errors in hypocenter location: Picking, model, and magnitude dependence. *Bulletin of the Seismological Society of America*, 84(6), 1978–1990. <https://doi.org/10.1785/bssa0840061978>
- Cai, C., Wiens, D. A., Shen, W., & Eimer, M. (2018). Water input into the Mariana Subduction Zone estimated from ocean-bottom seismic data. *Nature*, 563(7731), 389–392. <https://doi.org/10.1038/s41586-018-0655-4>
- Chapple, W. M., & Forsyth, D. W. (1979). Earthquakes and bending of plates at trenches. *Journal of Geophysical Research*, 84(B12), 6729–6749. <https://doi.org/10.1029/jb084ib12p06729>
- Christensen, D. H., & Ruff, L. J. (1988). Seismic coupling and outer rise earthquakes. *Journal of Geophysical Research*, 93(B11), 13421–13444. <https://doi.org/10.1029/jb093ib11p13421>
- Craig, T. J., & Copley, A. (2018). Forearc collapse, plate flexure, and seismicity within the downgoing plate along the Sunda Arc west of Sumatra. *Earth and Planetary Science Letters*, 484, 81–91. <https://doi.org/10.1016/j.epsl.2017.12.004>
- Craig, T. J., Copley, A., & Jackson, J. (2014). A reassessment of outer-rise seismicity and its implications for the mechanics of oceanic lithosphere. *Geophysical Journal International*, 197(1), 63–89. <https://doi.org/10.1093/gji/ggu013>
- Eimer, M., Wiens, D. A., Cai, C., Lizarralde, D., & Jaspersen, H. (2020). Seismicity of the incoming plate and forearc near the Mariana Trench recorded by ocean bottom seismographs. *Geochemistry, Geophysics, Geosystems*, 21(4), e2020GC008953. <https://doi.org/10.1029/2020gc008953>
- Emry, E. L., & Wiens, D. A. (2015). Incoming plate faulting in the Northern and Western Pacific and implications for subduction zone water budgets. *Earth and Planetary Science Letters*, 414, 176–186. <https://doi.org/10.1016/j.epsl.2014.12.042>
- Emry, E. L., Wiens, D. A., & Garcia-Castellanos, D. (2014). Faulting within the Pacific plate at the Mariana Trench: Implications for plate interface coupling and subduction of hydrous minerals. *Journal of Geophysical Research: Solid Earth*, 119(4), 3076–3095. <https://doi.org/10.1002/2013jb010718>
- Fisher, R. L. (1974). Pacific-type continental margins. In C. Burk & C. Drake (Eds.), *The geology of continental margins* (pp. 25–41). Springer.
- Fryer, P., Wheat, C., & Mottl, M. (1999). Mariana blueschist mud volcanism: Implications for conditions within the subduction zone. *Geology*, 27(2), 103–106. [https://doi.org/10.1130/0091-7613\(1999\)027<0103:mbmvif>2.3.co;2](https://doi.org/10.1130/0091-7613(1999)027<0103:mbmvif>2.3.co;2)
- Fujie, G., Kodaira, S., Yamashita, M., Sato, T., Takahashi, T., & Takahashi, N. (2013). Systematic changes in the incoming plate structure at the Kuril trench. *Geophysical Research Letters*, 40(1), 88–93. <https://doi.org/10.1029/2012gl054340>
- Grevemeyer, I., Ranero, C. R., Flueh, E. R., Kläschen, D., & Bialas, J. (2007). Passive and active seismological study of bending-related faulting and mantle serpentinization at the Middle America trench. *Earth and Planetary Science Letters*, 258(3–4), 528–542. <https://doi.org/10.1016/j.epsl.2007.04.013>
- Henza, A. A., Withjack, M. O., & Schlische, R. W. (2010). Normal-fault development during two phases of non-coaxial extension: An experimental study. *Journal of Structural Geology*, 32(11), 1656–1667. <https://doi.org/10.1016/j.jsg.2009.07.007>
- Hilde, T. W. C. (1983). Sediment subduction versus accretion around the Pacific. *Tectonophysics*, 99(2–4), 381–397. [https://doi.org/10.1016/0040-1951\(83\)90114-2](https://doi.org/10.1016/0040-1951(83)90114-2)
- Hsui, A. T., & Youngquist, S. (1985). A dynamic model of the curvature of the Mariana Trench. *Nature*, 318(6045), 455–457. <https://doi.org/10.1038/318455a0>
- Hunter, J., & Watts, A. (2016). Gravity anomalies, flexure and mantle rheology seaward of circum-Pacific trenches. *Geophysical Journal International*, 207(1), 288–316. <https://doi.org/10.1093/gji/ggw275>
- Ivandić, M., Grevemeyer, I., Bialas, J., & Petersen, C. J. (2010). Serpentinization in the trench-outer rise region offshore of Nicaragua: Constraints from seismic refraction and wide-angle data. *Geophysical Journal International*, 180(3), 1253–1264. <https://doi.org/10.1111/j.1365-246x.2009.04474.x>
- Jiao, W., Silver, P. G., Fei, Y., & Prewitt, C. T. (2000). Do intermediate- and deep-focus earthquakes occur on preexisting weak zones? An examination of the Tonga subduction zone. *Journal of Geophysical Research*, 105(B12), 28125–28138. <https://doi.org/10.1029/2000jb900314>
- Jones, G., Hilde, T., Sharman, G., & Agnew, D. (1978). Fault patterns in outer trench walls and their tectonic significance. *Journal of Physics of the Earth*, 26(Supplement), S85–S101. https://doi.org/10.4294/jpe1952.26.supplement_s85
- Kennett, B., & Engdahl, E. (1991). Traveltimes for global earthquake location and phase identification. *Geophysical Journal International*, 105(2), 429–465. <https://doi.org/10.1111/j.1365-246x.1991.tb06724.x>
- Klein, F. W. (2002). *User's guide to HYPOINVERSE-2000, a Fortran program to solve for earthquake locations and magnitudes*. US Geological Survey.
- Kobayashi, K., Cadet, J.-P., Aubouin, J., Boulègue, J., Dubois, J., vonHuene, R., et al. (1987). Normal faulting of the Daiichi-Kashima Seamount in the Japan Trench revealed by the Kaiko I cruise, Leg 3. *Earth and Planetary Science Letters*, 83(1–4), 257–266. [https://doi.org/10.1016/0012-821x\(87\)90070-7](https://doi.org/10.1016/0012-821x(87)90070-7)
- Lonsdale, P. (1988). Paleogene history of the Kula plate: Offshore evidence and onshore implications. *The Geological Society of America Bulletin*, 100(5), 733–754. [https://doi.org/10.1130/0016-7606\(1988\)100<0733:photkp>2.3.co;2](https://doi.org/10.1130/0016-7606(1988)100<0733:photkp>2.3.co;2)
- Lynnes, C. S., & Lay, T. (1988). Source process of the great 1977 Sumba earthquake. *Journal of Geophysical Research*, 93(B11), 13407–13420. <https://doi.org/10.1029/jb093ib11p13407>
- Masson, D. G. (1991). Fault patterns at outer trench walls. *Marine Geophysical Researches*, 13(3), 209–225. <https://doi.org/10.1007/bf00369150>
- McCaffrey, R., Molnar, P., Roecker, S. W., & Joyodiwiryo, Y. S. (1985). Microearthquake seismicity and fault plane solutions related to arc-continent collision in the eastern Sunda arc, Indonesia. *Journal of Geophysical Research*, 90(B6), 4511–4528. <https://doi.org/10.1029/jb090ib06p04511>

- Moberly, R. (1972). Origin of lithosphere behind island arcs, with reference to the western Pacific. In *Studies in Earth and space sciences* (pp. 35–55). A Memoir in Honor of Harry Hammond Hess.
- Moore, G. F., & Shipley, T. H. (1988). Mechanisms of sediment accretion in the Middle America trench off Mexico. *Journal of Geophysical Research*, 93(B8), 8911–8927. <https://doi.org/10.1029/jb093ib08p08911>
- Mousavi, S. M., Ellsworth, W. L., Zhu, W., Chuang, L. Y., & Beroza, G. C. (2020). Earthquake transformer—An attentive deep-learning model for simultaneous earthquake detection and phase picking. *Nature Communications*, 11, 1–12. <https://doi.org/10.1038/s41467-020-17591-w>
- Nakanishi, M., & Hashimoto, J. (2011). A precise bathymetric map of the world's deepest seafloor, Challenger Deep in the Mariana Trench. *Marine Geophysical Researches*, 32(4), 455–463. <https://doi.org/10.1007/s11001-011-9134-0>
- Oakley, A., Taylor, B., & Moore, G. (2008). Pacific Plate subduction beneath the central Mariana and Izu-Bonin fore arcs: New insights from an old margin. *Geochemistry, Geophysics, Geosystems*, 9(6), Q06003. <https://doi.org/10.1029/2007gc001820>
- Peacock, S. M. (2001). Are the lower planes of double seismic zones caused by serpentine dehydration in subducting oceanic mantle? *Geology*, 29(4), 299–302. [https://doi.org/10.1130/0091-7613\(2001\)029<0299:atlpod>2.0.co;2](https://doi.org/10.1130/0091-7613(2001)029<0299:atlpod>2.0.co;2)
- Pozgay, S. H., Wiens, D. A., Conder, J. A., Shiobara, H., & Sugioka, H. (2009). Seismic attenuation tomography of the Mariana subduction system: Implications for thermal structure, volatile distribution, and slow spreading dynamics. *Geochemistry, Geophysics, Geosystems*, 10(4), Q04X05. <https://doi.org/10.1029/2008gc002313>
- Pyle, M. L., Wiens, D. A., Weeraratne, D. S., Shore, P. J., Shiobara, H., & Sugioka, H. (2010). Shear velocity structure of the Mariana mantle wedge from Rayleigh wave phase velocities. *Journal of Geophysical Research*, 115, B11. <https://doi.org/10.1029/2009jb006976>
- Ranero, C. R., Morgan, J. P., McIntosh, K., & Reichert, C. (2003). Bending-related faulting and mantle serpentinization at the Middle America trench. *Nature*, 425(6956), 367–373. <https://doi.org/10.1038/nature01961>
- Ranero, C. R., Villaseñor, A., Phipps Morgan, J., & Weinrebe, W. (2005). Relationship between bend-faulting at trenches and intermediate-depth seismicity. *Geochemistry, Geophysics, Geosystems*, 6(12), Q12002. <https://doi.org/10.1029/2005gc000997>
- Renard, V., Nakamura, K., Angelier, J., Azema, J., Bourgois, J., Deplus, C., et al. (1987). Trench triple junction off Central Japan—Preliminary results of French-Japanese 1984 Kaiko cruise, Leg 2. *Earth and Planetary Science Letters*, 83(1–4), 243–256. [https://doi.org/10.1016/0012-821x\(87\)90069-0](https://doi.org/10.1016/0012-821x(87)90069-0)
- Shillington, D. J., Bécel, A., Nedimović, M. R., Kuehn, H., Webb, S. C., Abers, G. A., et al. (2015). Link between plate fabric, hydration and subduction zone seismicity in Alaska. *Nature Geoscience*, 8(12), 961–964. <https://doi.org/10.1038/ngeo2586>
- Shipley, T. H., & Moore, G. F. (1985). Sediment accretion and subduction in the Middle America trench. In N. Nasu, S. Kobayashi, S. Uyeda, I. Kushiro, & H. Kagami (Eds.), *Formation of active ocean margins* (pp. 221–225). Terra Scientific Publishing.
- Sleeper, J. D., Martinez, F., Fryer, P., Stern, R. J., Kelley, K. A., & Ohara, Y. (2021). Diffuse spreading, a newly recognized mode of crustal accretion in the southern Mariana Trough backarc basin. *Geosphere*, 17(5), 1382–1404. <https://doi.org/10.1130/ges02360.1>
- Stauder, W. (1968). Mechanism of the Rat Island earthquake sequence of February 4, 1965, with relation to island arcs and sea-floor spreading. *Journal of Geophysical Research*, 73(12), 3847–3858. <https://doi.org/10.1029/jb073i012p03847>
- Tichelaar, B. W., & Ruff, L. J. (1989). How good are our best models? Jackknifing, bootstrapping, and earthquake depth. *Eos, Transactions American Geophysical Union*, 70(20), 593–606. <https://doi.org/10.1029/89eo00156>
- Van Avendonk, H. J., Holbrook, W. S., Lizarralde, D., & Denyer, P. (2011). Structure and serpentinization of the subducting Cocos plate offshore Nicaragua and Costa Rica. *Geochemistry, Geophysics, Geosystems*, 12(6), Q06009. <https://doi.org/10.1029/2011gc003592>
- Waldhauser, F., & Ellsworth, W. L. (2000). *A Double-Difference Earthquake Location Algorithm: Method and Application to the Northern Hayward Fault, California* (Vol. 90, pp. 1353–1368). Bulletin of the Seismological Society of America.
- Wan, K., Lin, J., Xia, S., Sun, J., Xu, M., Yang, H., et al. (2019). Deep seismic structure across the southernmost Mariana Trench: Implications for arc rifting and plate hydration. *Journal of Geophysical Research: Solid Earth*, 124(5), 4710–4727. <https://doi.org/10.1029/2018jb017080>
- Ward, S. N. (1984). A note on lithospheric bending calculations. *Geophysical Journal International*, 78(1), 241–253. <https://doi.org/10.1111/j.1365-246x.1984.tb06482.x>
- Warsi, W. E., Hilde, T. W., & Searle, R. C. (1983). Convergence structures of the Peru Trench between 10 S and 14 S. *Tectonophysics*, 99(2–4), 313–329. [https://doi.org/10.1016/0040-1951\(83\)90110-5](https://doi.org/10.1016/0040-1951(83)90110-5)
- Yang, H., Zhu, L., & Chu, R. (2009). Fault-plane determination of the 18 April 2008 Mount Carmel, Illinois, earthquake by detecting and relocating aftershocks. *Bulletin of the Seismological Society of America*, 99(6), 3413–3420. <https://doi.org/10.1785/0120090038>
- Zhang, F., Lin, J., Zhou, Z., Yang, H., & Zhan, W. (2018). Intra- and intertrench variations in flexural bending of the Manila, Mariana and global trenches: Implications on plate weakening in controlling trench dynamics. *Geophysical Journal International*, 212(2), 1429–1449. <https://doi.org/10.1093/gji/ggx488>
- Zhang, J., Yang, H., Chen, H., Zhang, F., Zhu, G., & Sun, Z. (2020). Lateral change of in-plate stress and outer-rise seismicity along the southern Mariana trench. *Earth and Space Science Open Archive ESSOA*.
- Zhang, J., Zhang, F., Lin, J., & Yang, H. (2021). Yield failure of the subducting plate at the Mariana Trench. *Tectonophysics*, 814, 228944. <https://doi.org/10.1016/j.tecto.2021.228944>
- Zhang, J., Zhang, F., Yang, H., Lin, J., & Sun, Z. (2022). The effects of plateau subduction on plate bending, stress and intraplate seismicity. *Terra Nova*, 34(2), 113–122. <https://doi.org/10.1111/ter.12570>
- Zhang, M., Ellsworth, W. L., & Beroza, G. C. (2019). Rapid earthquake association and location. *Seismological Research Letters*, 90(6), 2276–2284. <https://doi.org/10.1785/0220190052>
- Zhou, Z., & Lin, J. (2018). Elasto-plastic deformation and plate weakening due to normal faulting in the subducting plate along the Mariana Trench. *Tectonophysics*, 734–735, 59–68. <https://doi.org/10.1016/j.tecto.2018.04.008>
- Zhou, Z., Lin, J., Behn, M. D., & Olive, J.-A. (2015). Mechanism for normal faulting in the subducting plate at the Mariana Trench. *Geophysical Research Letters*, 42(11), 4309–4317. <https://doi.org/10.1002/2015gl063917>
- Zhu, G., Wiens, D. A., Yang, H., Lin, J., Xu, M., & You, Q. (2021). Upper mantle hydration indicated by decreased shear velocity near the Southern Mariana Trench from Rayleigh wave tomography. *Geophysical Research Letters*, 48(15), e2021GL093309.
- Zhu, G., Yang, H., Lin, J., & You, Q. (2020). Determining the orientation of ocean-bottom seismometers on the seafloor and correcting for polarity flipping via polarization analysis and waveform modeling. *Seismological Research Letters*, 91(2A), 814–825. <https://doi.org/10.1785/0220190239>
- Zhu, G., Yang, H., Lin, J., Zhou, Z., Xu, M., Sun, J., & Wan, K. (2019). Along-strike variation in slab geometry at the Southern Mariana Subduction Zone revealed by seismicity through ocean bottom seismic experiments. *Geophysical Journal International*, 218(3), 2122–2135. <https://doi.org/10.1093/gji/ggz272>
- Zhu, L., & Helmlinger, D. V. (1996). Advancement in source estimation techniques using broadband regional seismograms. *Bulletin of the Seismological Society of America*, 86(5), 1634–1641. <https://doi.org/10.1785/bssa0860051634>
- Zhu, W., & Beroza, G. C. (2019). PhaseNet: A deep-neural-network-based seismic arrival-time picking method. *Geophysical Journal International*, 216, 261–273.

References From the Supporting Information

- Münchmeyer, J., Woollam, J., Rietbrock, A., Tilmann, F., Lange, D., Bornstein, T., et al. (2022). Which picker fits my data? A quantitative evaluation of deep learning based seismic pickers. *Journal of Geophysical Research: Solid Earth*, 127(1), e2021JB023499. <https://doi.org/10.1029/2021jb023499>
- Powers, D. M. (2020). *Evaluation: From precision, recall and F-measure to ROC, informedness, markedness and correlation*. arXiv preprint arXiv:2010.16061.
- Wong, W. C. J., Zi, J., Yang, H., & Su, J. (2021). Spatial-temporal evolution of injection-induced earthquakes in the Weiyuan Area determined by machine-learning phase picker and waveform cross-correlation. *Earth and Planetary Physics*, 5(6), 520–531.
- Zhou, P., Ellsworth, W. L., Yang, H., Tan, Y. J., Beroza, G. C., Sheng, M., & Chu, R. (2021). Machine-learning-facilitated earthquake and anthropogenic source detections near the Weiyuan Shale Gas Blocks, Sichuan, China. *Earth and Planetary Physics*, 5(6), 532–546. <https://doi.org/10.26464/epp2021053>
- Zhu, L., & Rivera, L. A. (2002). A note on the dynamic and static displacements from a point source in multilayered media. *Geophysical Journal International*, 148(3), 619–627. <https://doi.org/10.1046/j.1365-246x.2002.01610.x>